DTU Library

Improved Modeling Approaches for Constrained Sintering of Bi-Layered Porous Structures

Tadesse Molla, Tesfaye; Frandsen, Henrik Lund; Esposito, Vincenzo; Bjørk, Rasmus; Ni, De Wei; Olevsky, Eugene ; Pryds, Nini

Link back to DTU Orbit

Improved Modeling Approaches for Constrained Sintering of Bi-Layered Porous Structures

Tesfaye Tadesse Molla[1], Henrik Lund Frandsen[1], Vincenzo Esposito[1], Rasmus Bjørk[1], De Wei Ni[1], Eugene Olevsky[2], Nini Pryds[1]

[1]Department of Energy Conversion and Storage, Technical University of Denmark, Risø DTU campus,DK-4000 Roskilde, Denmark.
[2]Department of Mechanical Engineering, San Diego State University, San Diego, CA 92182-132,USA

Abstract

Shape instabilities during constrained sintering experiment of bi-layer porous and dense cerium gadolinium oxide (CGO) structures have been analyzed. An analytical and a numerical model based on the continuum theory of sintering has been implemented to describe the evolution of bow and densification kinetics in the sintering processes that consists of iso-rate and isothermal phases. The significant influence of weight of the sample (gravity) on the evolution of bow, especially in the isothermal sintering phase, is taken in to account. The modeling predictions indicate good agreement with the results of sintering of a bi-layered cerium-gadolinium oxide system in terms of evolution of bow, porosity and thickness.

Introduction

To improve the efficiency of membrane and solid oxide fuel cell technologies, it is often advantageous to increase the surface areas of the layers while decreasing their thickness. Sintering samples with such geometry is challenging, due to shape instabilities causing undesired distortion [1-4]. During sintering of multi-layer structures different densification rates can cause development of stresses leading to defects like cracks and macrostructural distortions [3-8]. Asymmetric arrangement of layers usually relaxes the mismatched stress evolutions by warping. Therefore there is a growing interest to understand how the intrinsic material properties can affect the evolution of distortion in order to reduce the stress development.

There have been a number of reported works that deal with distortions in bi-layer ceramic systems. One of these is the work by Chiang *et al.*[6], where a high and low dense borosilicate glass and alumina layers were co-fired to study the mismatch stress evolutions using the rate of bow development. Chiang *et al.* assumed the entire stress field to be due to the shrinkage rate difference. In addition, the stress and strain distributions along the section of the layers are known to be linear according to the beam theory, but in the model by Chiang *et al.* a uniform strain distributions are assumed over each layer, which could have affected the accuracy of the model.

Detailed work on experimental observation of processing defects and the corresponding viscoelastic stress computation for constrained densification of Alumina/Zirconia hybrid laminates has been published by Cai *et al.* [7, 8]. After measuring the viscous properties of the constituent layers using cyclic loading dilatometry, Cai *et al.* were able to model the bow evolution of bi-layers in good agreement with experimental results. Cai *et al.* however did not consider the evolution of thickness of each layer during densification, which is significant in case of highly porous layers.

In most of the works reported, the kinetics of densification and shape distortions are discussed either in the iso-rate or isothermal sintering phase with the relative differential shrinkage to be the factor controlling distortion [1-8, 16-22]. But the weight of the sample (gravity) also affects the rate of distortion by being an additional factor creating creep in the porous layers. Furthermore It is also necessary to develop a model for the entire sintering process consisting of the iso-rate and isothermal phases as is the actual practice. The work by Frandsen *et al.* [9], from which the basis for the modeling approach adopted in this study, is built on viscous analogy of classical laminate theory, where the effect of weight of the sample (gravity) on the distortion is also considered.

In this study, the experimental work reported by Esposito *et al.* [10] on tapes made from Cerium Gadolinium Oxides or CGO (Rhodia S.A.,France) with a specific surface area of 6.6 m^2/g (d50 particle size 0.2 μm) are used for demonstrations. Esposito *et al.* fabricated samples that consisted of two layers of CGO tape-casted on top of each other. One of the layers contained a significant amount of pre-calcined powder and graphite powder (V-UF1 99.9, Graphit Kropfmühl, Germany) as a pore former and will be referred to as CGO_P. The other layer has a higher density and will be referred to as CGO_D. The relative density and initial thickness of the porous layer was 18 vol% and 380 μm respectively. The corresponding dense layer was 48 vol% dense and 30 μm thick initially. The dense and porous tapes of length 24.5 mm and width 5.1 mm were laminated using screen printing. The samples were subsequently co-fired in a furnace with a temperature-time profile, which consists of constant rate firing with 0.83 K/min from 400°C to 1100°C followed by an isothermal sintering at 1100°C for 4 hours. Individual samples of each layer were also sintered in the same furnace in order to observe the free shrinkage of the each layer. The evolutions of

curvature in the bi-layer sample and shrinkage of the free samples were recorded *in-situ* using a high temperature furnace equipped with an optical dilatometer (Fraunhofer-Institute Silicateforschung, Germany).

The objective of this study is to present an improved way of modeling bow evolution during the entire sintering of porous and dense layers of CGO ($Ce_{0.9}$ $Gd_{0.1}$ $O_{1.95-d}$) where the effect of gravity on the distortion evolution is considered to be another stress generating factor in addition to the differential shrinkage. Furthermore a linear distribution of strain with the evolution of thickness across each layer has also been considered. The same approach is also implemented numerically based on 3D finite element technique.

Co-sintering Model

The analysis is made based on continuum theory of sintering, which relates the external load to the strain rate by nonlinear viscous constitutive relationship [11, 12] as shown in Eq. (1).

$$\sigma_{ij} = 2\eta_0\left[\varphi\dot{\varepsilon}_{ij} + \left(\psi - \frac{1}{3}\varphi\right)\dot{e}\delta_{ij}\right] + P_L\delta_{ij} \tag{1}$$

where η_0 is the shear viscosity of the fully dense materials, φ and ψ are the normalized shear and bulk viscosities, P_L is the effective driving potential for sintering or sintering stress, δ_{ij} the Kronecker symbol and $\dot{\varepsilon}_{ij}$ and $\dot{e}$ are the shear and bulk strain rates respectively related to the stress tensor σ_{ij}. The normalized shear and bulk viscosities are considered to be function of porosity, θ. The effective sintering stress is a function of surface energy per unit area (α) and grain size (G) in the form shown by Eq. (2).

$$P_L = \frac{3\alpha}{2G}f_1(\theta) \tag{2}$$

where $f_1(\theta)$ is time dependent function of porosity. The porosity evolution is related to the volumetric densification strain using the principles of mass conservation as [6]:

$$\dot{e} = \frac{\dot{\theta}}{1 - \theta} \tag{3}$$

For detailed description of the continuum theory of sintering, especially of its microstructural assumptions, $f_1(\theta)$, please refer to Olevsky [11, 12].

The shear viscous properties of the fully dense bodies are assumed to vary with temperature (T) and the instantaneous grain size (G) in each layer according to Eq. (4). [23]

$$\eta_0 = AG^3\exp\left(\frac{E_s}{RT}\right) \tag{4}$$

Where A is the pre-exponential constant in the Arrhenius type of viscosity function, E_s is the apparent activation energy for sintering and R is the universal gas constant.

The simultaneous coarsening or grain growth during the sintering process is considered to be a function of time, t, limited by the activation energy for grain growth (E_g) as shown in Eq.(5) [13, 24]. Here n is the grain growth exponent depending on the creep or diffusion mechanism (e.g. $n = 2$ for Nabarro-Herring creep and $n = 3$ for Coble creep) and k_o is the pre-exponential constant [13].

$$G^n = G_0^n + k_0\exp\left(\frac{-E_g}{RT}\right)t \tag{5}$$

(1)   Stresses in bi-layer system

The stresses developed in the bi-layer system that lead to bending of the sample are assumed to be because of two phenomena occurring simultaneously during co-firing. These are the relative difference in shrinkage rate of the two layers and creep due to stresses from own weight (gravity) of the sample.

As shown by the schematics of a sectioned bi-layer system in Fig. 1a, the relative difference in the rate of shrinkage between a porous thick layer and dense thin layer creates the densification mismatch, which leads to an in-plane force ($\acute{N}$) and the bending moment ($\acute{M}$). For the sample geometry the stress normal to the interface is very small compared to the in-plane stresses. So the relative difference in shrinkage generates a biaxial state of sintering stress and a bending moment that bends the sample towards the porous layer. This phenomenon can be considered as a creep process due to the internal sintering stress, where the biaxial stress is linearly related to the viscosity of the porous body (E_b'), which is given by $E_b' = \eta_0 f_2(\theta)$ [9]. In this work, positive curvature is defined when the sample bows towards the porous layer.
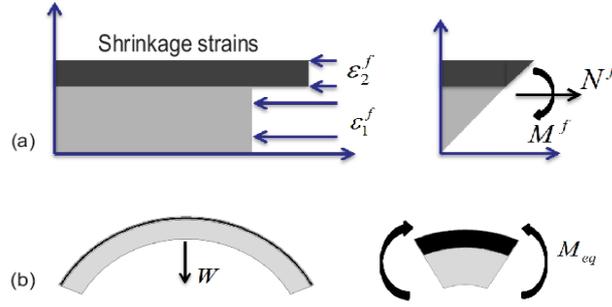
Fig.1: Schematics showing stress in sintering of bi-layer structure (a) due to relative difference in shrinkage & (b) due to creep because of own weight.

Creep because of the own weight (W) of the entire body (gravity), while it sinters is also another phenomena generating stresses in the bi-layer structure. Unlike creep due to the internal sintering stress, which deforms the structure towards the porous layer, creep due to the weight of the body tends to oppose the deformation (e.g. negative curvature). The reason for this is explained schematically in Fig. 1b. Since the width of the sample is small compared to its length, the structure can be considered as a beam with evenly distributed weight over its length. Therefore, the creep generates only a uniaxial state of stress due to the equivalent bending moment (M_{eq}) which opposes the deformation of the sample. Here also the uniaxial stress is considered to be linearly proportional to the viscosity of the porous body (E'_u), given by $E'_u = \eta_0 f_3(\theta)$ [9].

(2) Kinetics of shrinkage and distortion

In this work, linear distribution of the constrained strain rate across the section of each layer is assumed. This is achieved by using the viscous analogy of classical laminate theory with the evolving curvature rate ($\dot{\kappa}$) and longitudinal strain rate ($\dot{\varepsilon}_0$) to describe the linear strain rate distribution ($\dot{\varepsilon}$) over the thickness of the beam as shown in Eq. (8) with z representing the vertical coordinate of a point in the layer.

$$\dot{\varepsilon} = \dot{\varepsilon}_0 + \dot{\kappa} z \tag{6}$$

The corresponding distribution of stress is also linear with the generalized material viscosity (E'), which depends on the evolving viscosity of porous body, see Eq. (9), and the difference between the constrained ($\dot{\varepsilon}$) and free shrinkage rates ($\dot{\varepsilon}^f$) [9].

$$E' = \begin{cases} E'_b & \text{for biaxial stress} \\ E'_u & \text{for uniaxial stress} \end{cases} \tag{7}$$

$$\sigma = E'\dot{\varepsilon}' = E'(\dot{\varepsilon} - \dot{\varepsilon}^f) = E'(\dot{\varepsilon}_0 + \dot{\kappa} z - \dot{\varepsilon}^f) \tag{8}$$

Further theoretical details of the model described above and the derived microstructural time dependent functions f_2 and f_3 can be found in Frandsen *et al.* [9]. The free shrinkage rates are calculated directly from Eq. (1) using the effective sintering stress, P_L as:

$$\dot{\varepsilon}^f = -\frac{P_L}{6\eta_0 \psi} \tag{9}$$

The longitudinal strain rates ($\dot{\varepsilon}_0$) and curvature rate ($\dot{\kappa}$) are evaluated by integrating stresses and the bending moments in both layers as [9]:

$$\int_{\text{both layers}} \sigma dz = 0 \tag{10}$$

$$\int_{\text{both layers}} \sigma z dz = 0 \tag{11}$$

Thereby solving the constrained strain rate ($\dot{\varepsilon}$) with the help of Eq. (8) for the coordinate point defined by z. The evolving porosity (θ) and the thickness (h) of each layer in the bi-layer sample are also updated through time considering the total stress states in each layer during the co-firing. The above approaches are used to solve two parallel problems simultaneously accounting for the biaxial stresses due to differential shrinkage and the uniaxial stresses due to weight of the sample (gravity).

The curvature evolution due to the weight of the sample was approximated by assuming a constant equivalent bending moment (M_{eq}) [9]. The total curvature rate was then calculated simulating the simultaneous effects in the same co-ordinate system.

All the information for shrinkages and bow development can be integrated through time according to the sintering profile used in the experiment if the viscosities of both layers at fully dense state (η_{01}, η_{02}), the corresponding surface energies (α_1, α_2) and the grain growth kinetics in each layer (G_1, G_2) are known.

(3) Obtaining the constitutive parameters

In this work, an alternative approach to experimentations has been employed to find the material parameters required for modeling the shrinkage and camber development observed during the entire sintering process. This is achieved through first modeling the shrinkage and camber development behaviors during isothermal sintering period using the procedures explained in section III. For the isothermal sintering, it is assumed that the viscosity of the fully dense materials and grain sizes remain constant. This assumption is fairly reasonable for a constant temperature regime as supported by Kanters *et al*. [3]. Having the grain size at the holding temperature (e.g. G_1, G_2), the model described in Section III can be implemented using Matlab to find the shrinkage strains and curvature evolutions. The model predictions for curvature (κ) and free strains ($\dot{\varepsilon}^f$) evolutions in each layer can be optimized with the respective experimental data. This can be done by starting the model simulations with realistic guesses of the four unknown constitutive parameters of each layer i.e. (η_{01}, η_{02}) and (α_1, α_2). The unknown constitutive parameters can then be identified as those providing the minimum deviation as per Eq. (12) between the experimental data and model simulation.

$$\Delta = \left\{ \sum_{i=1}^{N} \left[\left(\frac{\kappa^{Sim} - \kappa^{Exp}}{mean(\kappa^{Exp})} \right)^2 + \left(\frac{\varepsilon_1^{f,Sim} - \varepsilon_1^{f,Exp}}{mean(\varepsilon_1^{f,Exp})} \right)^2 + \left(\frac{\varepsilon_2^{f,Sim} - \varepsilon_2^{f,Exp}}{mean(\varepsilon_2^{f,Exp})} \right)^2 \right] \right\}^{\frac{1}{2}} \quad (12)$$

where κ and ε^f are the curvature and free shrinkage strains in each layer respectively and the sum taken over all N data points in time. For a sintering profile that constitutes an iso-rate followed by isothermal sintering, the grain sizes at the holding temperature (e.g. G_1, G_2) and at the onset of the iso-rate sintering (e.g. G_{01}, G_{02}), could be used to estimate the grain growth pre-exponential factors (k_{01}, k_{02}), see Eq. (5), using experimentally determined activation energies for grain growth [14]. This would help to approximate the grain growth kinetics in the two layers during the iso-rate sintering process as per Eq. (5). Similarly, the viscosities estimated for fully dense layers at the holding temperatures using the optimization above, see Eq.(12), can be used to calculate the constants (A_1, A_2), see Eq.(4). This could approximate the viscosity function for the entire sintering process as per the temperature variation with the help of experimentally determined apparent activation energy for densification [14]. The details of the optimization procedure to find the basic material parameters at the holding temperature together with SEM micrograph measurements of porosity and the various assumptions taken can be found elsewhere [15].

Results and Discussions

Fig.2 shows a SEM image of a section of the bi-layer laminate after sintering. Note that there were no sintering defects such as cracks or de-lamination in the interface of the CGO_P and CGO_D layers, which is one of the requirements for the classical laminate theory.

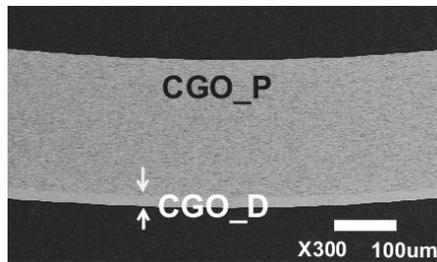

Fig. 2: Cross sectional SEM images of the microstructures:
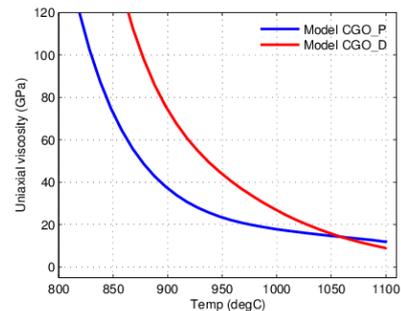CGO_D and CGO_P with no defects

Fig. 3: Viscosity evolutions during the iso-rate sintering

The evolutions of uniaxial viscosities of the porous layers as a function of temperature as per Eq. (4) are shown in the Fig. 3. The trend in the evolution of viscosity is consistent with the one reported by Ewsuk et *al*.[16] showing the influences of

temperature at the beginning and evolving density at higher temperatures. Table 1 summarizes the different parameters used in the modeling of the entire sintering process.

Table 1: Material parameters used to model the entire sintering process

Parameter	CGO_P	CGO_D	Source
Apparent activation energy for densification (kJ/mol)	430	430	[14]
Activation energy for grain growth (kJ/mol)	413	430	[14]
Initial grain size, G_0 (μm)	0.4	0.25	[10]
Grain size at holding temperature (μm)	1.25	1.25	Estimated
Initial porosity level (%)	77	42	[10]
Initial thickness (μm)	380	30	[10]
Arrhenius constants (Pa.s/m^3)	7.5×10^{11}	1.3×10^{11}	Fitted
Grain growth pre-exponential factors (m^3/s)	2.1×10^{-7}	4.5×10^{-7}	Fitted

Fig. 4 shows the comparison between experiment and model for the densifications in terms of shrinkage strains in the free sintering samples during the entire sintering times. The porous layer is shown to shrink by around 40% while the dense layer shrunk by approximately 20%. Shrinkage in the dense layer is also observed to bypass the shrinkage in the porous layer for a few range of time in the sintering process. The model also shows a good agreement with experimentally observed shrinkages in both CGO_P and CGO_D layers.

Fig. 5 shows the experimentally observed bow development throughout the entire sintering process in comparison with the model prediction. The model captured the development of the bow towards the dense layer due to the faster shrinkage in the CGO_D before it is reversed to the porous layer. The effect of gravity is again shown to be significant during the last stage of the sintering mainly in the isothermal sintering. But the influence of gravity in the iso-rate sintering period is shown to be very small as the comparison between the models used in this study to the one by Cai *et al.* reflects (see Fig. 5).
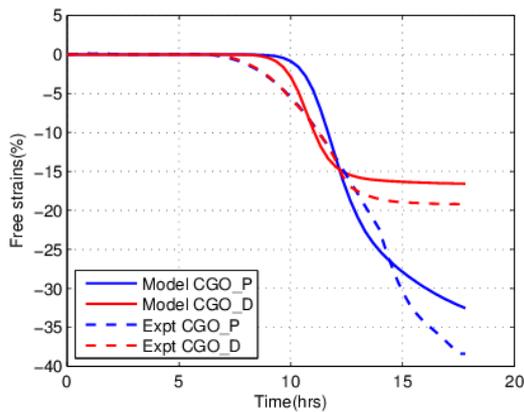

Fig. 4: Comparison of the model to the experimental data for free shrinkage strains during the entire sintering
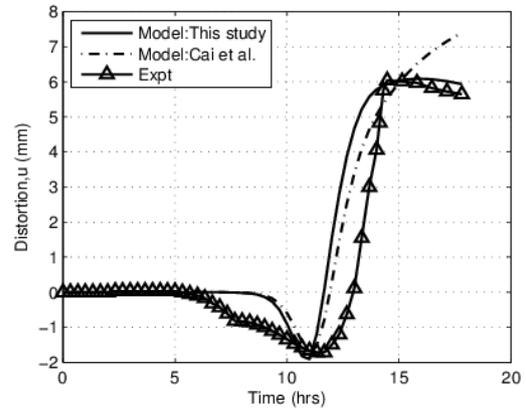
Fig. 5: Comparison of the model to the experimental data for distortion (u) during the entire sintering

Apart from predicting the bow development, the model estimations of the final porosity and thickness are also in a good agreement with the results measured from the SEM studies, see Fig. 6. As expected, the porosity of the CGO_P layer shows a fast and large reduction compared with the reduction of the dense layer, CGO_D. The model also predicts a similar trend in the evolution of thickness with the CGO_P layer showing a large reduction and almost no reduction in thickness for the CGO_D layer. Again the final thickness results predicted by the model correspond well with the experimental data as shown in Fig. 7.
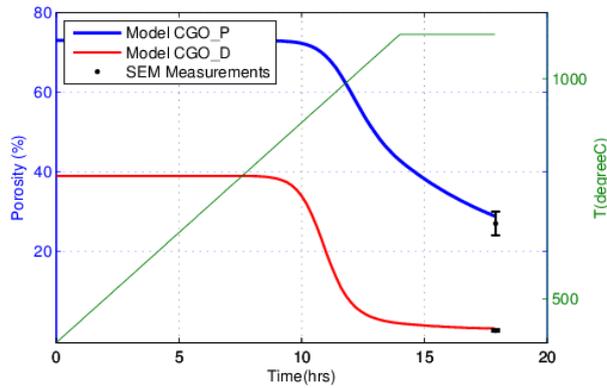
Fig. 6: Model predictions of porosity evolutions throughout the sintering process and SEM measurements at the end of the entire sintering.
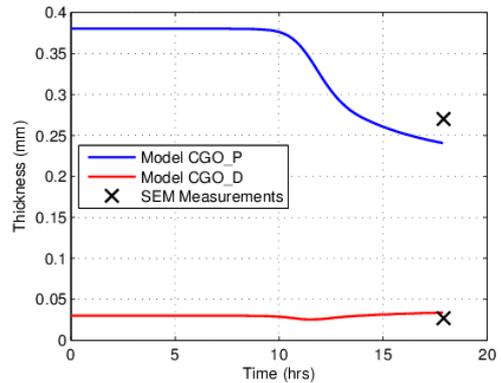

Fig. 7: Model predictions of thickness evolutions throughout the sintering process and SEM measurements at the end of the entire sintering.

Apart from the analytical model, a numerical model is also being developed based on the continuum theory of sintering explained in section III using the commercial finite element program COMSOL 4.3. A user defined creep formulation is coupled with evolution equations for porosity to solve for the displacement fields on symmetrical model geometry. The 3D model is intended to capture the geometrical features which were not captured by the analytical model like the curvature across the width of the sample. Fig. 8 show the 3D image of the distortion observed at the end of the sintering process from an ongoing work on numerical model based on finite element methods. Fig.9 also shows the corresponding sample after the sintering experiment. The distortion is shown to be large around the edges of the sample which is found to be consistent with the experimental observations of the bi-layer system.
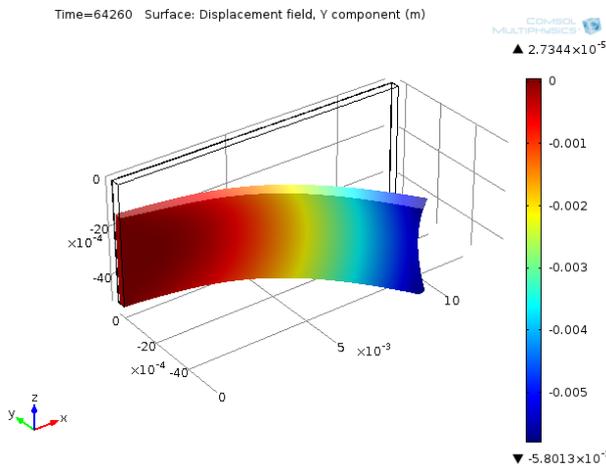

Fig. 8: 3D finite element result for distortion at the end of the sintering process

Fig. 9: Image of distortion of bi-layered system after the entire sintering experiment

Conclusions

Experimentally observed behaviors of shrinkage and bow development during sintering of bi-layer sample of porous and dense cerium gadolinium oxide (CGO) layers were studied. It was possible to get an improved prediction from model implemented by considering the effect of gravity on the distortion and using linear distribution of strain rates across the section of each layer together with the evolving thickness. The bi-layer was observed to have a reduced deformation rate mainly in the isothermal sintering, as is observed experimentally. The reason for this was deducted to be due to gravity, because the free sintering samples sintered throughout the experiment. But the influence of gravity, in the experiment considered, is shown to be minimal in the iso-rate sintering stage as there are high amount of sintering activity in the porous layer. The complete

geometrical feature of the distorted sample after the sintering experiment were also modeled numerically and found to be consistent with the experiments.

The effect of gravity could be studied further by varying the length of the samples. Also the effect of porosity which varies along the sintering strip according to the variable stress state could also be studied further.

References

[1]. R. Muecke, N. Menzler, H. Buchkremer and D. Stoever, 'Co-firing of Thin Zirconia Films During SOFC Manufacturing', *J Am Ceram Soc*, 92[1] (2009) S95-S102.

[2]. H. Li, C. Xia, X. Fang, X. He, X. Wei and G. Meng ,'Co-sintering of SDC/NiO-SDC bi-layers prepared by tape casting', *High-Performance Ceramics, Pts 1 and 2*, (2005) 280-283 779-784.

[3]. J. Kanters, U. Eisele and J. Rodel, 'Cosintering simulation and experimentation: Case study of nanocrystalline zirconia,' *J Am Ceram Soc*, 84 [12] (2001) 2757-2763.

[4]. J. Chang, O. Guillon, J. Roedel and S. L. Kang, 'Characterization of warpage behaviour of Gd-doped ceria/NiO-yttria stabilized zirconia bi-layer samples for solid oxide fuel cell applications', *J. Power Sources*, 185 [2] (2008)759-764.

[5]. G. Lu, R. Sutterlin and T. Gupta, 'Effect of Mismatched Sintering Kinetics on Camber in a Low-Temperature Cofired Ceramic Package', *J Am Ceram Soc*, 76 [8] (1993)1907-1914.

[6]. M. Chiang, J. Jean and S. Lin, 'Effects of green density difference on camber development during the cofiring of a bi-layer glass-based dielectric laminate', *Mater. Chem. Phys*., 128 [3] 413-417 (2011).

[7]. P. Cai, D. Green and G. Messing, 'Constrained densification of alumina/zirconia hybrid laminates .1. Experimental observations of processing defects', *J Am Ceram Soc*, 80 [8] (1997) 1929-1939.

[8]. P. Cai, D. Green and G. Messing, 'Constrained densification of alumina/zirconia hybrid laminates .2. Viscoelastic stress computation', *J Am Ceram Soc*, 80 [8] (1997)1940-1948.

[9]. H. Frandsen, E. Olevsky, T. Molla, V. Esposito, R. Bjørk, N. Pryds, 'Modeling sintering of multilayers under the influence of gravity', *J Am Ceram Soc*,2012 (*Accepted*)

[10]. V. Esposito, E. Olevsky, D. Ni, R. Bjørk, N. Pryds, 'Sintering of bi-layered porous structures', *J Am Ceram Soc*, (*unpublished*)

[11]. E. Olevsky, 'Theory of sintering: from discrete to continuum,' *Materials Science & Engineering R-Reports*, 23 [2] (1998) 41-100.

[12]. E. Olevsky, V. Tikare and T. Garino, 'Multi-scale study of sintering: A review', *J Am Ceram Soc*, 89 [6] (2006) 1914-1922.

[13]. F. Raether, P. Schulze, 'Investigation of sintering mechanism of alumina using kinetic field and master sintering diagram', J Eur Ceram Soc,29 (2009) 2225-2234

[14]. D. Ni, V. Esposito, C. Schmidt, S. Ramousse, N. Pryds, 'Densification kinetics analysis of CGO and LSM/CGO tape casting layers',(*unpublished*)

[15]. T. Molla, H. Frandsen, V. Esposito, R. Bjørk, D. Ni, E. Olevsky, N. Pryds, 'Modeling kinetics of distortion in porous bi-layered structures under the influence of gravity', *J Eur Ceram Soc*, (*unpublished*)

[16]. M. Reiterer, K. Ewsuk,'An Arrhenius-type viscosity function to model sintering using the Skorohod-Olevsky viscous sintering model within a finite element code', *J Am Ceram Soc*, 89 [6] (2006) 1930-1935.

[17]. J. Lu, H. Hng, X. Song, T. Zhang and J. Ma, 'Cosintering of a Bimodal Pore Distribution Layered Structure: Constitutive Models and Experiments RID A-2246-2011', *J Am Ceram Soc*, 94 [5] (2011) 1528-1535.

[18]. D. Ravi and D. Green, 'Sintering stresses and distortion produced by density differences in bi-layer structures', *J Eur Ceram Soc*, 29 [8] (2009) 1547-1547.

[19]. A. Atkinson, J. Kim, R. Rudkin, S. Taub and X. Wang, 'Stress Induced by Constrained Sintering of 3YSZ Films Measured by Substrate Creep', *J Am Ceram Soc*, 94 [3] (2011) 717-724.

[20]. F. Raether, R. Springer and S. Beyer, 'Optical dilatometry for the control of microstructure development during sintering', *Mater Res Innovations*, 4 [4] (2001) 245-250.

[21]. R. Hsu and J. Jean, 'Key factors controlling camber behavior during the cofiring of bi-layer ceramic dielectric laminates', *J Am Ceram Soc*, 88 [9] (2005) 2429-2434.

[22]. J. Ollagnier, O. Guillon and J. Roedel, 'Constrained Sintering of a Glass Ceramic Composite: I. Asymmetric Laminate', *J Am Ceram Soc*, 93 [1] (2010) 74-81.

[23]. M.Delporte, 'A phenomenological approach to the prediction of material behaviours during co-sintering', *PhD thesis*, Würzburg, 2009, pp.84-85

[24]. M.Rahaman, 'Sintering of ceramics' *1st ed.*, CRC press: Taylor & Francis Group, 2008, pp.122-124